CrystEngComm

PAPER

View Article Online
View Journal | View Issue

Cite this: *CrystEngComm*, 2014, **16**, 7598

Synthesis, structure, and piezoelectric properties of ferroelectric and antiferroelectric $NaNbO_3$ nanostructures†

Shaozheng Ji,[a] Hong Liu,*[ab] Yuanhua Sang,[a] Wei Liu,[a] Guangwei Yu[a] and Yanhua Leng[a]

Received 31st May 2014, Accepted 20th June 2014

DOI: 10.1039/c4ce01116c

www.rsc.org/crystengcomm

$NaNbO_3$ cubes and nanowires have been synthesized by a hydrothermal-based method utilizing thin Nb foil and low-concentration NaOH solution with the presence of H_2O_2. The $Na_2Nb_2O_6 \cdot H_2O$ precursor can be obtained under hydrothermal conditions at 200 °C for only 4 h. Both long-time hydrothermal treatment and calcination on the precursor nanowires can realize the transition from $Na_2Nb_2O_6 \cdot H_2O$ nanowires to $NaNbO_3$ crystalline particles. However, the crystalline phases of the two products are different. $NaNbO_3$ microcubes obtained by long-time hydrothermal treatment are in the antiferroelectric phase with space group *Pbma*, while $NaNbO_3$ nanowires obtained by annealing $Na_2Nb_2O_6 \cdot H_2O$ at 500 °C for 3 h are in the ferroelectric phase with space group $P2_1ma$. The experimental results from X-ray diffraction (XRD), field emission scanning electron microscopy (FESEM), high resolution electron microscopy (HRTEM) and Raman spectroscopy proved the difference between the crystalline phases of $NaNbO_3$ microcubes and nanowires. Piezoelectric force microscopy (PFM) analysis proved that $NaNbO_3$ nanowires exhibit piezoelectricity, while no piezoelectric response can be detected for $NaNbO_3$ microcubes synthesized by direct hydrothermal treatment.

Introduction

Alkaline niobates are very important functional materials due to their piezoelectricity, pyroelectricity, electro-optic, photovoltaic effect, nonlinear optical response and photocatalytic properties.[1–5] As one of the important members of this group, sodium niobate ($NaNbO_3$) has attracted much attention recently because of the exceptional piezoelectric response in $NaNbO_3$-derived ceramics, which is a promising lead-free alternative to the widely used lead-based piezoelectric ceramics $Pb(Zr_xTi_{1-x})O_3$(PZT).[6] $NaNbO_3$ and $NaNbO_3$-derived nanocrystals[7–9] have been widely studied and were found to have applications as photocatalysts[10,11] and piezoelectric nanogenerators.[12] Furthermore, the polymorphism of $NaNbO_3$ based on its perovskite structure is quite complicated, and to determine the close relationship between its crystalline structure and functional properties, many researchers have studied the influence of temperature, crystal size and other parameters on its crystalline structure.[13–17]

$NaNbO_3$ single crystals and ceramics at room temperature are commonly recognized to have an antiferroelectric phase with an orthorhombic unit cell, space group *Pbma*. In a study by Shuvaeva and co-workers,[18] $NaNbO_3$ in the antiferroelectric phase can be induced to the ferroelectric phase by application of a sufficient external electric field. Its unit cell is orthorhombic in the polar space group $P2_1ma$ with parameters a = 5.569 Å, b = 7.790 Å, and c = 5.518 Å. Shiratori *et al.*[19] reported that the phase transition can also be induced by the particle size. Johnston *et al.*[13] compared the solid-state preparation, molten salt preparation and sol–gel preparation products, and concluded that the synthetic route heavily influences both the crystal structure and the microstructure.

$NaNbO_3$ powders have been synthesized by traditional solid-state techniques, the hydrothermal method, the microemulsion-mediated approach, the solvothermal method and so on.[20–23] The hydrothermal method has been proven to be simple, mild and cost-effective. Nb_2O_5 and high-concentration NaOH are generally utilized as the starting reagents.[22,24] Nb powder[25] and $Nb(OC_2H_5)_5$ (ref. 20) were also chosen as the Nb-sources. In this paper, quite thin niobium foil with 0.05 mm thickness and low-concentration NaOH were chosen as the starting materials. The reaction process and structure evolution under hydrothermal conditions were studied in detail. Two types of $NaNbO_3$ powders, $NaNbO_3$

[a] *State Key Laboratory of Crystal Materials, Shandong University, 27 Shandanan Road, Jinan, 250100, China. E-mail: hongliu@sdu.edu.cn*
[b] *Beijing Institute of Nanoenergy and Nanosystems, Chinese Academy of Science, Beijing 100864, PR China*

† Electronic supplementary information (ESI) available: See DOI: 10.1039/c4ce01116c

microcubes and $NaNbO_3$ nanowires, were obtained by the hydrothermal process. Because of the polymorphism of $NaNbO_3$, X-ray diffraction and Rietveld refinement were utilized to analyse the crystalline structures of $NaNbO_3$ microcubes and $NaNbO_3$ nanowires. Raman spectroscopy and piezoelectric force microscopy (PFM) were carried out to provide evidence clarifying the difference between these two types of $NaNbO_3$. It was found that $NaNbO_3$ microcubes are in the antiferroelectric phase with the space group *Pbma*, while $NaNbO_3$ nanowires are in the ferroelectric phase with the space group $P2_1ma$. The ferroelectric $NaNbO_3$ nanowires may have applications in future devices such as data storage memories, energy harvesting devices and electromechanical systems.

Experimental procedure

Sample preparation

The starting materials, sodium hydroxide (NaOH) and hydrogen peroxide (H_2O_2, 30%) were purchased from Sinopharm Chemical Reagent Co., Ltd, China, and are of AR grade without any purification. Metallic niobium foil (Nb, 99.99%) with a thickness of 0.05 mm was chosen as the Nb source in this experiment. Nb foil was cleaned with alcohol by sonication for 15 min. $Na_2Nb_2O_6{\cdot}H_2O$ nanowires were firstly prepared by a hydrothermal method. In a typical synthesis process, a piece of thin Nb foil (20 mm × 10 mm × 0.05 mm) was placed in the bottom of a Teflon-lined autoclave (capacity, 25 ml). 5–17 ml of 2.0 M NaOH solution with 2 ml of H_2O_2 (30%) was then added into the autoclave. The sealed autoclave was kept in an electric oven for 4 h at 200 °C. The obtained white precipitate was dispersed in deionized water by an ultrasonic treatment for 30 min, rinsed with deionized water 3 times, and dried at 60 °C overnight. There are two methods to synthesize $NaNbO_3$ particles from $Na_2Nb_2O_6{\cdot}H_2O$ nanowires. One is to prolong the hydrothermal treatment time to transform $Na_2Nb_2O_6{\cdot}H_2O$ into $NaNbO_3$. In order to study the transformation process, the products were all obtained by hydrothermal treatment for 8 h, 12 h and 24 h. The other approach uses $Na_2Nb_2O_6{\cdot}H_2O$ nanowires as precursor and obtains $NaNbO_3$ nanowires by careful calcination. Typically, $NaNbO_3$ nanowires could be obtained by annealing the precursor at 500 °C for 3 h.

Characterization

Field emission scanning electron microscopy (FESEM, Model JSM-7600F, JEOL Ltd., Tokyo, Japan) was used to characterize the morphology and size of the synthesized samples. High-resolution transmission electron microscopy (HRTEM) images were obtained with a JOEL JEM 2100F microscope. X-ray powder diffraction (XRD) patterns were recorded on a Bruker D8 Advance powder X-ray diffractometer with Cu Kα (λ = 0.15406 nm). TG/DTA characterization was done using a Diamond TG/DTA analyzer (Perkin Elmer). Raman spectroscopy was carried out using a Jobin-Yvon HR 800 spectrometer with a 473-nm excitation laser. IR spectra were obtained using a Nicolet FTIR760 infrared spectrometer. Piezoelectric force microscopy (PFM) was performed using a Bruker Dimension Icon Scanning Probe Microscope with a Pt-coated conductive tip. In order to measure the piezoelectric property of the powder sample, the powders were firstly dispersed in alcohol and then dropped on an Au-coated silicon wafer. The prepared sample was kept in a 200 °C electric oven for 2 h to fix the powder on the surface of the silicon wafer.

Rietveld refinements were carried out on the powder XRD data using the General Structure Analysis System (GSAS) program and EXPGUI front-end[26,27] with the structural information from the X-ray powder diffraction data as the starting point. The high-intensity XRD data were obtained by slow scan speed (1 s per step with a step length of 0.02°) from 15° to 120° using a Bruker D8 Advance powder X-ray diffractometer. A pseudo-Voigt function (GSAS type #4) was used as the profile function for the XRD data sets. Rietveld refinements of the model in the space groups $P2_1ma$ and *Pbma* were carried out using the models of Shuvaeva[18] and Xu *et al.*,[28] respectively.

Results and discussion

The XRD patterns of the products obtained by hydrothermal treatment at 200 °C for 4–24 h are shown in Fig. 1. In Fig. 1(a), all of the peaks in the XRD pattern can be indexed as peaks of $Na_2Nb_2O_6{\cdot}H_2O$. $Na_2Nb_2O_6{\cdot}H_2O$ is the end member of Sandia octahedral molecular sieves (SOMS) which are a new class of octahedral microporous phases with the composition $Na_2Nb_{2-x}M_xO_{6-x}(OH)_x{\cdot}H_2O$($M$ = Ti, Zr; $0 < x \leq 0.4$) and have a framework structure composed of $[NbO_6]$, $[MO_6]$, and $[NaO_6]$ octahedra linked by corner or edge sharing.[29–31] When the hydrothermal reaction time was increased to 8 h, the XRD pattern in Fig. 1(b) shows that most of the peaks attributed to $Na_2Nb_2O_6{\cdot}H_2O$ disappear except for four small

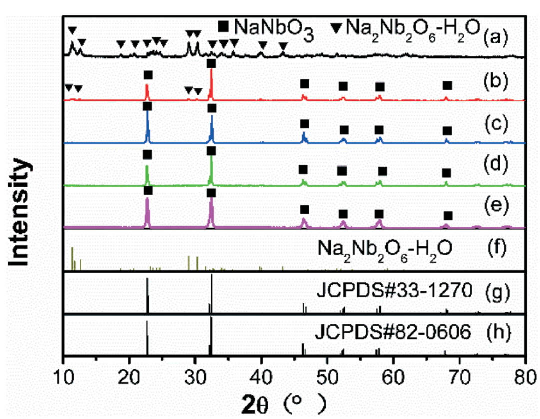

Fig. 1 XRD patterns of products synthesized under hydrothermal conditions for (a)4 h, (b)8 h, (c)12 h, and (d)24 h and (e) the calcined product obtained by annealing the 4-h product at 500 °C for 3 h. Pattern (f) is the standard diffraction pattern of $Na_2Nb_2O_6{\cdot}H_2O$. Patterns (g) and (h) correspond to the standard diffraction patterns of $NaNbO_3$ in the *Pbma* space group and $NaNbO_3$ in the $P2_1ma$ space group, respectively.

peaks. The new peaks with high intensity can be indexed as the peaks of $NaNbO_3$, which means that $NaNbO_3$ with good crystallinity is formed. When the hydrothermal time was further prolonged to 12 h, all of the peaks can be indexed to $NaNbO_3$ without any of them attributed to $Na_2Nb_2O_6\cdot H_2O$ as shown in Fig. 1(c). When the hydrothermal time was increased to 24 h, the product exhibits no phase change anymore. Patterns (g) and (h) in Fig. 1 show the standard diffraction patterns of $NaNbO_3$ in the *Pbma* (JCPDS#33-1207) and *P*2$_1$*ma* space groups (JCPDS#82-0606), respectively. These two diffraction patterns are similar, making it hard to index the accurate crystalline structure of the hydrothermal products. However, from the phase evolution shown in Fig. 1, it can be concluded that $Na_2Nb_2O_6\cdot H_2O$ is metastable under hydrothermal conditions. With increasing hydrothermal time, the precursor molecules lose combined water and are converted into $NaNbO_3$. After the 12-h hydrothermal treatment, pure $NaNbO_3$ can be obtained.

TG/DTA measurement on the $Na_2Nb_2O_6\cdot H_2O$ powder was performed in air from room temperature to 750 °C to investigate its stability and predict the phase transition during the heating treatment. The obtained curve is shown in Fig. 2. There is an endothermic peak at 265 °C. The corresponding weight loss is ~4.2%. This is close to the ideal value of 5.2% weight percent of combined water based on the formula $Na_2Nb_2O_6\cdot H_2O$. Thus, the endothermic peak at 265 °C is due to the loss of combined water. An exothermic peak appears at 475 °C without weight loss which arises from the transition of $Na_2Nb_2O_6$ to its dense form.[29] When $Na_2Nb_2O_6\cdot H_2O$ was annealed at 500 °C for 3 h, $NaNbO_3$ was obtained as shown in Fig. 1(e). It can be seen that the product has good crystallographic quality. When $Na_2Nb_2O_6\cdot H_2O$ was annealed at 300 °C or 400 °C for 3 h, $NaNbO_3$ could not be formed (Fig. S1 of the ESI†). This is in agreement with the TG/DTA curve of $Na_2Nb_2O_6\cdot H_2O$. When comparing the XRD patterns of $NaNbO_3$ obtained by long-time hydrothermal treatment (Fig. 1(d)) with those of $NaNbO_3$ obtained by annealing $Na_2Nb_2O_6\cdot H_2O$ (Fig. 1(e)), no obvious difference could be observed. A detailed discussion will be shown later to confirm their accurate crystalline structures.

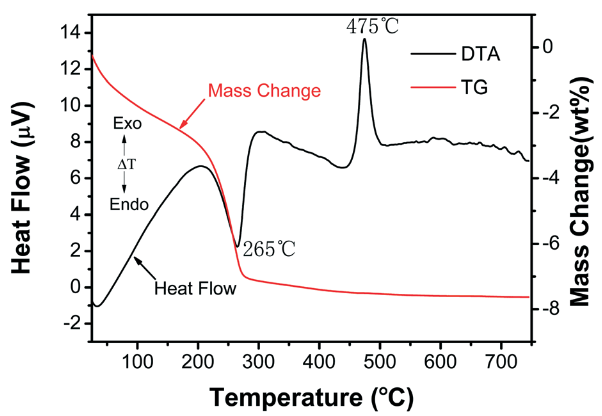

Fig. 2 TG/DTA curve of $Na_2Nb_2O_6\cdot H_2O$.

IR spectra of the hydrothermal products and products obtained by annealing $Na_2Nb_2O_6\cdot H_2O$ at 500 °C are shown in Fig. 3. In Fig. 3(a), the peaks at 3207.9 cm^{-1} and 3369.1 cm^{-1} correspond to the vibration of O–H. The peak at 1696.7 cm^{-1} can be attributed to the H–O–H bending of the molecular water. The absorption bands located below 1000 cm^{-1} are vibrations of the Na-niobate framework including M–O stretching, M–O–M bending (M = Nb, Na), and lattice vibrations.[30] With the increasing hydrothermal time, the intensity of the peaks at 3207.9 cm^{-1}, 3369.1 cm^{-1} and 1696.7 cm^{-1} decreases until it disappears completely after the 24-h hydrothermal treatment. It can be inferred that the amount of water in the hydrothermal products decreases gradually until it disappears with the increasing hydrothermal time. In the range below 1000 cm^{-1}, the divided adsorption peaks broaden gradually to a wider absorption range with increasing hydrothermal time corresponding to the phase transition from $Na_2Nb_2O_6\cdot H_2O$ to $NaNbO_3$. The IR spectra of the 24-h hydrothermal product (Fig. 3(d)) and the calcined $NaNbO_3$ product (Fig. 3(e)) are almost the same, which means that the 24-h hydrothermal product is pure $NaNbO_3$ without $Na_2Nb_2O_6\cdot H_2O$. The evolution of IR spectra proves that during the hydrothermal process $Na_2Nb_2O_6\cdot H_2O$ loses combined water and transforms to $NaNbO_3$ ultimately, which agrees well with the XRD result.

Morphological observation on the samples of different hydrothermal times and the calcined product obtained by annealing $Na_2Nb_2O_6\cdot H_2O$ at 500 °C is shown in Fig. 4. The 4-h product is a $Na_2Nb_2O_6\cdot H_2O$ nanowire of 10–20 μm in length and about 150 nm in width as shown in Fig. 4(a, b). Delamination at the end of one $Na_2Nb_2O_6\cdot H_2O$ nanowire is shown in Fig. 4(c). The boundary coming from different layers at the end is clear, which may signify the layerered structure of $Na_2Nb_2O_6\cdot H_2O$. The 8-h product shown in Fig. 4(d) is the mixture of micro-sized irregular blocks and nanowires. The surface of blocks is rough, covering some nanowires. Fewer nanowires appear in the 12-h product as shown in Fig. 4(e), and micro-sized regular cubes with a

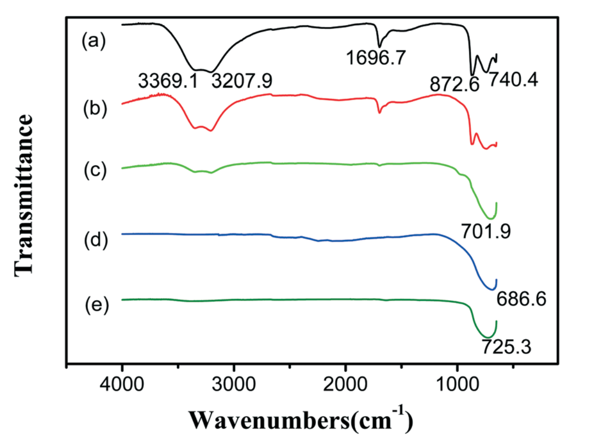

Fig. 3 IR spectra of products synthesized under hydrothermal conditions for (a)4 h, (b)8 h, (c)12 h, and (d)24 h and (e) the calcined product obtained by annealing the 4-h product at 500 °C for 3 h.

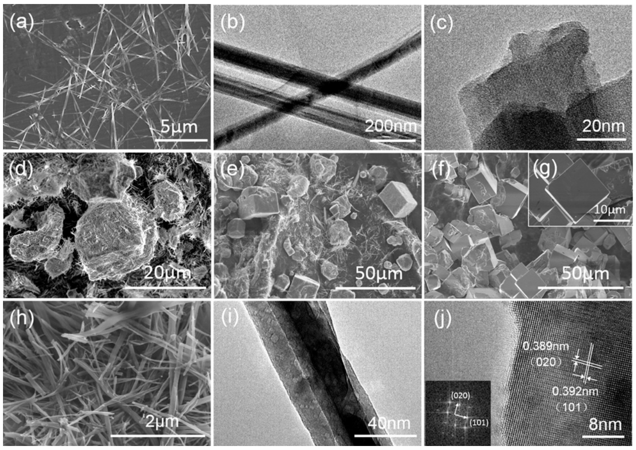

Fig. 4 (a) SEM image of $Na_2Nb_2O_6{\cdot}H_2O$ obtained by the 4 h hydrothermal treatment. (b), (c) HRTEM images of the $Na_2Nb_2O_6{\cdot}H_2O$ nanowire. Images (d), (e), and (f) are SEM images of 8 h, 12 h and 24 h hydrothermal treatment products, respectively. Image (g) is the partial enlargement of image (f). Image (h) is the SEM image of the product obtained by annealing $Na_2Nb_2O_6{\cdot}H_2O$ precursor nanowires. Images (i) and (j) are the HRTEM images of product synthesized by annealing the $Na_2Nb_2O_6{\cdot}H_2O$ precursor nanowires. The inset in image (j) is the fast Fourier transform (FFT) pattern for $NaNbO_3$.

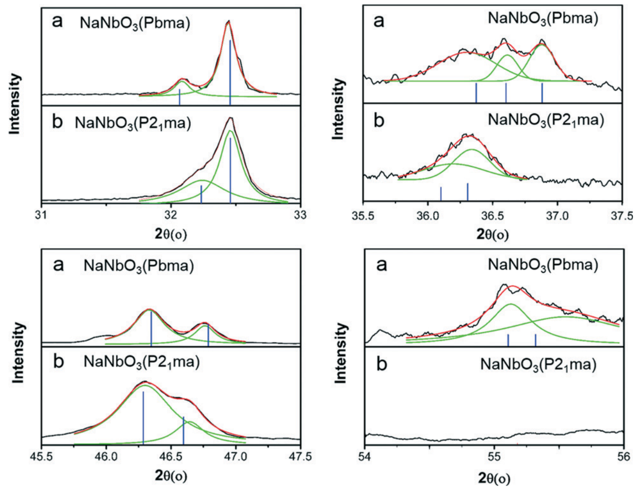

Fig. 5 a: XRD patterns of $NaNbO_3$ synthesized by the 24 h hydrothermal treatment. b: XRD patterns of $NaNbO_3$ obtained by annealing the $Na_2Nb_2O_6{\cdot}H_2O$ precursor. The four images show the difference of their XRD patterns in the ranges 31°–33°, 35.5°–37.5°, 45.5–47.5°, 54–56°. The blue lines show the position and relative intensity of the standard diffraction peaks.

smooth surface begin to appear. In Fig. 4(f), all of the particles synthesized for 24 hours by hydrothermal treatment are micro-sized cubes with some cubes embedded into their neighbor, and the surface of the cubes is smooth as shown in Fig. 4(g). The transformation mechanism from $Na_2Nb_2O_6{\cdot}H_2O$ nanowires to $NaNbO_3$ cubes can be found in ref. 17. $Na_2Nb_2O_6{\cdot}H_2O$ dissolves to provide the source of $[NbO_6]$ or clusters of $[NbO_6]$ for the growth of the $NaNbO_3$ cubes. FESEM and HRTEM images of the calcined product formed by annealing the $Na_2Nb_2O_6{\cdot}H_2O$ precursor at 500 °C for 3 h are shown in Fig. 4(h) and (i, j), respectively. The calcined $NaNbO_3$ basically keeps the nanowire morphology with about 50 nm width as shown in Fig. 4(i). The lattice structure of calcined $NaNbO_3$ is shown in Fig. 4(j). The $NaNbO_3$ nanowire has high crystalline quality evidenced by clear lattice fringes. The interplanar spacings are 0.389 nm and 0.392 nm in two perpendicular directions. The inset in Fig. 4(j) is the fast Fourier transform (FFT) image of $NaNbO_3$ which shows its orthorhombic crystalline structure.

As mentioned above, $NaNbO_3$ nanowires obtained by annealing the $Na_2Nb_2O_6{\cdot}H_2O$ precursor and $NaNbO_3$ microcubes synthesized by prolonging the hydrothermal treatment time may have different crystalline structures. To recognize the difference in the crystalline structures between the two products, XRD patterns with high intensity were obtained from the two samples, and the lattice parameters were obtained by Rietveld refinements. In Fig. 1, the XRD patterns of the powder product synthesized under hydrothermal conditions for 24 hours and the product obtained by annealing the $Na_2Nb_2O_6{\cdot}H_2O$ precursor look the same. However, if we enlarge the XRD patterns, there are some obvious differences which are shown in Fig. 5. In the ranges 31°–33° and 45.5°–47.5°, there are two diffraction peaks both for $NaNbO_3$ synthesized by the 24 h hydrothermal treatment and that synthesized by annealing the $Na_2Nb_2O_6{\cdot}H_2O$ precursor, which agreed well with the two standard JCPDS cards no. 33-1270 (*Pbma*) and no. 86-0606($P2_1ma$), respectively. In the range of 35.5°–37.5°, there are three peaks for $NaNbO_3$ synthesized by the 24 h hydrothermal treatment while there are only two peaks for $NaNbO_3$ obtained by annealing the $Na_2Nb_2O_6{\cdot}H_2O$ precursor, which also agreed with the two JCPDS cards. In the range 54°–56°, $NaNbO_3$ synthesized by the 24 h hydrothermal treatment has a diffraction peak while that obtained by annealing the $Na_2Nb_2O_6{\cdot}H_2O$ precursor has none. From these features, $NaNbO_3$ synthesized by the 24 h hydrothermal treatment can be indexed to JCPDS no. 33-1270 (*Pbma*) while $NaNbO_3$ obtained by annealing the $Na_2Nb_2O_6{\cdot}H_2O$ precursor can be indexed to JCPDS no. 86-0606($P2_1ma$). The former has an antiferroelectric phase and the latter has a ferroelectric structure. In order to further confirm their phase structures, Rietveld refinements for $NaNbO_3$ synthesized by the 24 h hydrothermal treatment and $NaNbO_3$ obtained by annealing the $Na_2Nb_2O_6{\cdot}H_2O$ precursor were carried out based on the structures of JCPDS no. 33-1270 and no. 86-0606, respectively. The refinement results are shown in Fig. 6, showing an excellent agreement between observed and calculated patterns. The insets in Fig. 6(a) and (b) are the unit cells of $NaNbO_3$ in *Pbma* and $P2_1ma$, respectively. The unit cell of *Pbma* $NaNbO_3$ in Fig. 6(a) displays an unusual "octahedral tilting" scheme with three independent tilts leading to a $\sqrt{2}a_p \times \sqrt{2}a_p \times 4a_p$ supercell of the basic cubic perovskite subcell, where a_p is the idealized cubic perovskite lattice parameter. Compared with *Pbma* $NaNbO_3$, $NaNbO_3$ in $P2_1ma$ has a smaller unit cell described by $\sqrt{2}a_p \times \sqrt{2}a_p \times 2a_p$ as shown in the inset of Fig. 6(b).[13] In contrast to $NaNbO_3$ in *Pbma*, the lack of b slip

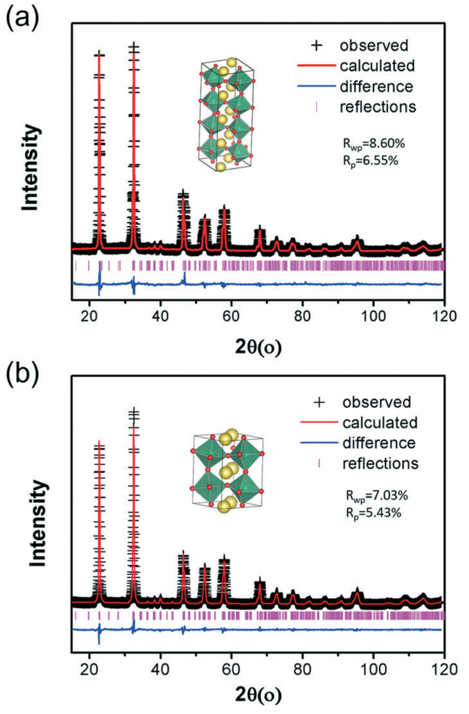

Fig. 6 Fitted XRD patterns of (a) $NaNbO_3$ synthesized by the 24 h hydrothermal treatment and (b) $NaNbO_3$ obtained by annealing the $Na_2Nb_2O_6 \cdot H_2O$ precursor. Plus (+) symbols represent the measured results and the solid line is from refinement. The difference between observed and calculated results is shown beneath (blue). The insets in Fig. 6(a) and (b) are the unit cells of $NaNbO_3$ in *Pbma* and $P2_1ma$ symmetry, respectively. Yellow and red balls represent Na and O atoms, respectively. The green octahedron represents the $[NbO_6]$ unit.

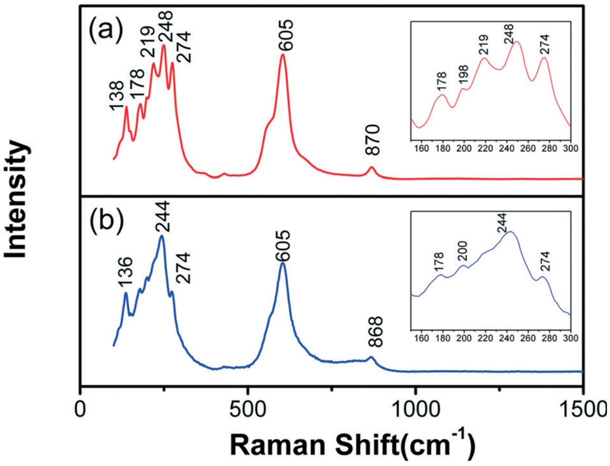

Fig. 7 Raman spectra of (a) $NaNbO_3$ synthesized by the 24 h hydrothermal treatment and (b) $NaNbO_3$ obtained by annealing the $Na_2Nb_2O_6 \cdot H_2O$ precursor. The insets are the enlarged parts from 150 cm^{-1} to 300 cm^{-1}.

in $P2_1ma$ makes it a noncentrosymmetrical phase exhibiting a spontaneous polarization which is the necessary condition for piezoelectric and ferroelectric properties. The refined unit cell parameters and atom corporation are listed in Table S1 and S2 of the ESI.† The interplanar spacings of 0.389 nm and 0.392 nm in Fig. 4(j) correspond to the crystal planes (020) and (101) of $NaNbO_3$ in $P2_1ma$, respectively.

Raman spectroscopy is sensitive to the octahedral tilting associated with the $NaNbO_3$ phase structure. Therefore, Raman spectra were recorded to further prove the difference of these two samples under 473 nm laser excitation. The obtained Raman spectra are shown in Fig. 7. A remarkable difference between the spectra in Fig. 7(a) and (b) can be observed within the region between 150 cm^{-1} and 300 cm^{-1}, as shown in the insets of Fig. 7(a) and (b). In this range, the spectrum in Fig. 7(a) shows obvious splitting peaks compared with the spectrum in Fig. 7(b). The peak at 219 cm^{-1} in Fig. 7(a) almost disappears in Fig. 7(b) and the location of the highest peak has a small shift. All of the bands in the range 150–1000 cm^{-1} are associated with the internal vibrational modes of NbO_6. The region from 150 to 300 cm^{-1} is related to the triply degenerate ν_6 (F2u) and ν_5 (F2g) modes.[15,20] The spectrum of $NaNbO_3$ obtained by annealing the $Na_2Nb_2O_6 \cdot H_2O$ precursor agrees well with the $P2_1ma$ phase reported in ref. 14. Raman spectroscopy further proved the structural difference of $NaNbO_3$ synthesized by the 24 h hydrothermal treatment and by annealing the $Na_2Nb_2O_6 \cdot H_2O$ precursor.

It is well known that only noncentrosymmetrical crystal structures can exhibit piezoelectric properties. Thus, the $NaNbO_3$ nanowires obtained by annealing the $Na_2Nb_2O_6 \cdot H_2O$ precursor with a noncentrosymmetrical crystal structure can exhibit piezoelectric properties in theory, while $NaNbO_3$ microcubes synthesized by the 24 h hydrothermal treatment cannot. Piezoelectric force microscopy (PFM) is a common technique for the study of ferroelectric and piezoelectric phenomena in low dimensional materials.[32–34] Therefore, in this work, piezoelectric responses of the two samples were characterized by PFM. After the application of a 10 V AC voltage on the conductive tip of the PFM, the piezoelectric response of the $NaNbO_3$ nanowire obtained by annealing the $Na_2Nb_2O_6 \cdot H_2O$ precursor is shown in Fig. 8. Fig. 8(a) depicts the height image of a single $NaNbO_3$ nanowire. Fig. 8(b) and (c) show the amplitude and phase maps of the piezoelectric response, respectively. The amplitude and phase images agree well with each other. In ref. 20, Tsung-Ying Ke *et al.* also observed the piezoelectric properties of a $NaNbO_3$ nanowire. The piezoelectric properties of the $NaNbO_3$ nanowire obtained by annealing the $Na_2Nb_2O_6 \cdot H_2O$ precursor further confirm its noncentrosymmetrical crystal structure. Furthermore, by applying a ramp voltage loop from −10 to 10 V and then reversing to the dashed rectangular region in Fig. 8(b), the standard ferroelectric butterfly amplitude curve (Fig. 8(d)) and phase curve (Fig. 8(e)) were obtained. This is the most important evidence that the $NaNbO_3$ nanowire exhibits typical ferroelectric properties. For $NaNbO_3$ microcubes synthesized by the 24 h hydrothermal treatment, PFM was also used to detect their piezoelectric properties. As mentioned earlier, the size of $NaNbO_3$ microcubes is too large to measure the piezoelectric properties using PFM. To realize the PFM measurement, the $NaNbO_3$ cubes were ground to smaller particles, dispersed in ethanol, and fixed on an

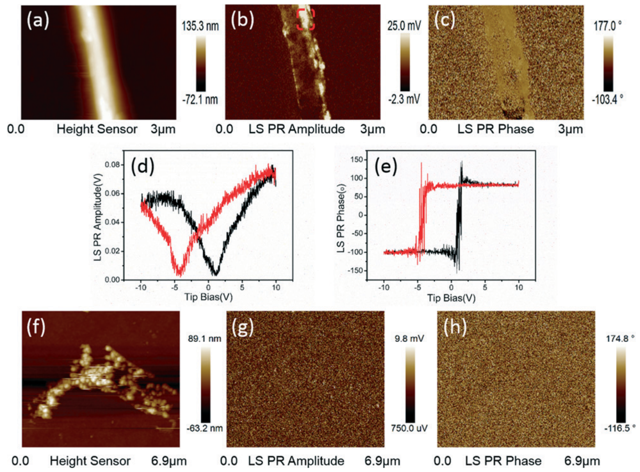

Fig. 8 (a) Height image of a $NaNbO_3$ nanowire obtained by annealing the $Na_2Nb_2O_6{\cdot}H_2O$ precursor. (b) The relative amplitude of piezoelectric response and (c) the phase of piezoelectric response. By applying ramp voltage from −10 to 10 V and then reversing to the dashed rectangular region in amplitude image (b), the standard ferroelectric amplitude curve (d) and the phase curve (e) were obtained. (f) The height image of the $NaNbO_3$ powder obtained by the 24 h hydrothermal treatment. (e) The relative amplitude of piezoelectric response and (f) the phase of piezoelectric response.

Au-coated silicon wafer using the procedure described in the experimental section. The SEM image with the morphology of ground particles is shown in Fig. S2 of the ESI.† The average size of the particles is about 300 nm. Under the same experimental conditions, there is no piezoelectric response observed as shown in Fig. 8(g) and (h), which agrees with its centrosymmetric crystalline structure.

Conclusions

In summary, we have successfully and efficiently synthesized $Na_2Nb_2O_6{\cdot}H_2O$ nanowires by a hydrothermal method utilizing thin Nb foil as the Nb-source at a low concentration of NaOH solution with the presence of H_2O_2. When the hydrothermal treatment time is prolonged under the same hydrothermal conditions, $Na_2Nb_2O_6{\cdot}H_2O$ can lose combined water and ultimately transform into $NaNbO_3$ microcubes. $NaNbO_3$ nanowires can be obtained by annealing $Na_2Nb_2O_6{\cdot}H_2O$ nanowires at 500 °C. $NaNbO_3$ microcubes and $NaNbO_3$ nanowires have different crystalline structures corresponding to an antiferroelectric crystal structure with the *Pbma* space group and a ferroelectric phase with the $P2_1ma$ space group, respectively. Because of the noncentrosymmetrical crystalline structure, $NaNbO_3$ nanowires exhibiting piezoelectric properties may be applied in data storage memories, energy harvesting devices and nanoelectromechanical systems.

Acknowledgements

This research was supported by the Natural Science Foundation of China (grant no. 51372142, 21071090), the National Science Fund for Distinguished Young Scholars (NSFDYS: 50925205), Innovation Research Group (IRG: 51321091) and the "100 Talents Program" of the Chinese Academy of Sciences.

Notes and references

1 Y. Nakayama, P. J. Pauzauskie, A. Radenovic, R. M. Onorato, R. J. Saykally, J. Liphardt and P. Yang, *Nature*, 2007, **447**, 1098–1101.
2 F. Dutto, C. Raillon, K. Schenk and A. Radenovic, *Nano Lett.*, 2011, **11**, 2517–2521.
3 M. Nyman, F. Bonhomme, T. M. Alam, M. A. Rodriguez, B. R. Cherry, J. L. Krumhansl, T. M. Nenoff and A. M. Sattler, *Science*, 2002, **297**, 996–998.
4 Q. P. Ding, Y. P. Yuan, X. Xiong, R. P. Li, H. B. Huang, Z. S. Li, T. Yu, Z. G. Zou and S. G. Yang, *J. Phys. Chem. C*, 2008, **112**, 18846–18848.
5 I. Grinberg, D. V. West, M. Torres, G. Gou, D. M. Stein, L. Wu, G. Chen, E. M. Gallo, A. R. Akbashev, P. K. Davies, J. E. Spanier and A. M. Rappe, *Nature*, 2013, **503**, 509–512.
6 E. Cross, *Nature*, 2004, **432**, 24–25.
7 L. Q. Cheng, K. Wang, Q. Yu and J. F. Li, *J. Mater. Chem. C*, 2014, **2**, 1519–1524.
8 Y. Xu, Q. Yu and J. F. Li, *J. Mater. Chem.*, 2012, **22**, 23221–23226.
9 Z. Wang, H. S. Gu, Y. M. Hu, K. Yang, M. Z. Hu, D. Zhou and J. G. Guan, *CrystEngComm*, 2010, **12**, 3157–3162.
10 K. Saito and A. Kudo, *Inorg. Chem.*, 2010, **49**, 2017–2019.
11 P. Li, S. Ouyang, Y. J. Zhang, T. Kako and J. H. Ye, *J. Mater. Chem. A*, 2013, **1**, 1185–1191.
12 J. H. Jung, M. Lee, J.-I. Hong, Y. Ding, C.-Y. Chen, L.-J. Chou and Z. L. Wang, *Acs Nano*, 2011, **5**, 10041–10046.
13 K. E. Johnston, C. C. Tang, J. E. Parker, K. S. Knight, P. Lightfoot and S. E. Ashbrook, *J. Am. Chem. Soc.*, 2010, **132**, 8732–8746.
14 S. K. Mishra, R. Mittal, V. Y. Pomjakushin and S. L. Chaplot, *Phys. Rev. B: Condens. Matter Mater. Phys.*, 2011, **83**, 134105.
15 Z. X. Shen, X. B. Wang, M. H. Kuok and S. H. Tang, *J. Raman Spectrosc.*, 1998, **29**, 379–384.
16 K. K. Mishra, V. Sivasubramanian and A. K. Arora, *J. Raman Spectrosc.*, 2011, **42**, 517–521.
17 S. K. Mishra, M. K. Gupta, R. Mittal, S. L. Chaplot and T. Hansen, *Appl. Phys. Lett.*, 2012, **101**, 242907.
18 V. A. Shuvaeva, M. Y. Antipin, R. S. V. Lindeman, O. E. Fesenko, V. G. Smotrakov and Y. T. Struchkov, *Ferroelectrics*, 1993, **141**, 307–311.
19 Y. Shiratori, A. Magrez, W. Fischer, C. Pithan and R. Waser, *J. Phys. Chem. C*, 2007, **111**, 18493–18502.
20 Y. Shiratori, A. Magrez, J. Dornseiffer, F.-H. Haegel, C. Pithan and R. Waser, *J. Phys. Chem. B*, 2005, **109**, 20122–20130.
21 J. Koruza, J. Tellier, B. Malič, V. Bobnar and M. Kosec, *J. Appl. Phys.*, 2010, **108**, 113509.
22 H. Y. Zhu, Z. F. Zheng, X. P. Gao, Y. N. Huang, Z. M. Yan, J. Zou, H. M. Yin, Q. D. Zou, S. H. Kable, J. C. Zhao, Y. F. Xi, W. N. Martens and R. L. Frost, *J. Am. Chem. Soc.*, 2006, **128**, 2373–2384.

23 Q. L. Gu, K. J. Zhu, J. S. Liu, P. C. Liu, Y. Cao and J. H. Qiu, *RSC Adv.*, 2014, **4**, 15104–15110.
24 T. Y. Ke, H. A. Chen, H. S. Sheu, J. W. Yeh, H. N. Lin, C. Y. Lee and H. T. Chiu, *J. Phys. Chem. C*, 2008, **112**, 8827–8831.
25 L. Liu, B. Li, D. H. Yu, Y. M. Cui, X. F. Zhou and W. P. Ding, *Chem. Commun.*, 2010, 427–429.
26 A. C. Larson and R. B. V. Dreele, *Los Alamos National Laboratory Report LAUR*, 1994, p. 86.
27 B. Toby, *J. Appl. Crystallogr.*, 2001, **34**, 210–213.
28 H. W. Xu, Y. L. Su, M. L. Balmer and A. Navrotsky, *Chem. Mater.*, 2003, **15**, 1872–1878.
29 H. W. Xu, M. Nyman, T. M. Nenoff and A. Navrotsky, *Chem. Mater.*, 2004, **16**, 2034–2040.
30 M. Nyman, A. Tripathi, J. B. Parise, R. S. Maxwell and T. M. Nenoff, *J. Am. Chem. Soc.*, 2002, **124**, 1704–1713.
31 M. Nyman, A. Tripathi, H. B. Parise, R. S. Maxwell, W. T. A. Harrison and T. M. Nenoff, *J. Am. Chem. Soc.*, 2001, 1529–1530.
32 A. Gruverman, D. Wu and J. Scott, *Phys. Rev. Lett.*, 2008, **100**, 097601.
33 G. Suyal, E. Colla, R. Gysel, M. Cantoni and N. Setter, *Nano Lett.*, 2004, **4**, 1339–1342.
34 M. H. Zhao, Z. L. Wang and S. X. Mao, *Nano Lett.*, 2004, **4**, 587–590.

